Arch. Mech., **55**, 5–6, pp. 501–514, Warszawa 2003

Numerical simulation of atomic positions in quantum dot by means of molecular statics

P. DŁUŻEWSKI, P. TRACZYKOWSKI

Institute of Fundamental Technological Research, PAS
Świętokrzyska 21, 00-049 Warsaw
*e-mail:*pdluzew@ippt.gov.pl
*e-mail:*ptracz@ippt.gov.pl

Deformation of a crystal structure is considered here in terms of constitutive modelling based upon both the atomistic and continuum approaches. Atomistic calculations are made by using the Stillinger–Weber potential for the GaAs and CdTe structures. The stress-strain behaviour of the best-known anisotropic hyperelastic models are compared with the behaviour of the atomistic one in the uniaxial deformation test.

Key words: molecular simulations, stress analysis, nonlinear elasticity, molecular potential, Stillinger–Weber potential, finite element analysis.

1. Introduction

Recently many molecular models of crystal behaviour have been used in modelling of the crystal lattice deformation. Many constitutive models based on the continuum thermodynamics are also available. Hence the question arises about the relation between the nonlinear behaviour of these two types of models. For instance, it is well known that the stress-strain behaviour of nonlinear continuum elastic models depends very heavily on the strain measure applied, [1, 4]. Namely, the linear stress-strain constitutive relation rewritten for the stress conjugate to the Almansi strain makes the extension softer than compression, while the analogical linear stress-strain constitutive relation for the second Piola–Kirchhoff stress conjugate by work with the Green strain measure makes the extension harder than compression. It is easy to show on the third order elastic constants obtained by reducing these nonlinear constitutive equation to the common strain measures, e.g. to the logarithmic strain [4].

Atomistic modelling of crystal deformation can be divided into the computational methods based upon the fundamental and empirical potentials. The fundamental potentials are based upon the quantum theory and Schrödinger wave equation, while the empirical potentials predict the dependence of strain energy directly on the basis of atomic positions. It can be shown that the quasi-classical

treatment of atomic interaction in terms of interatomic potentials and the classical momentum equation are consistent in certain limits with the solution of the Schrödinger wave equation [8, 3]. The analogy results from the decomposition of the analytical solution into the time-dependent and time-independent parts. The time-independent wave function corresponds to the spatial arrangement of particles. Generally, the empirical potentials can be divided into two and more modern many-body potentials. In the simple pair potentials (like the Morse, Lennard–Jones, Madelung ones) only the direct interaction of two atoms is considered and added up for a certain sphere with the radius of about four atoms. In the multi-atom potentials not only two-atoms but also the influence of the neighbouring atoms is taken into account; for example, in the Stillinger–Weber potentials applied here noncentral atomic interactions are taken into account by adding three-atoms interaction terms.

Continuum models of elastic behaviour of crystal lattice can be divided generally into the linear models based on the linear theory of elasticity, and nonlinear constitutive models where the differentiation of displacement field over the current and initial configurations are distinguished. In the linear theory, by writing $\varepsilon_{ij} = \frac{1}{2}(\nabla_i u_j + \nabla_j u_i)$ we do not specify precisely over which configuration the differentiation is made, i.e. over the current or the initial configuration. Generally, we assume then that it does not matter because the configuration changes are very small. In the nonlinear theory, before the displacement gradient is written, we have to answer precisely over which configuration the differentiation is done.

Anisotropic hyperelastic models compose a very narrow group among numerous continuum models describing elastic behaviour of materials. Let us emphasize that the most familiar *anisotropic* hyperelastic models, like the St.-Venant–Kirchhoff and Biot models, change heavily their instantaneous stiffness under large strains. Moreover, the stiffness evolution often differs significantly from the behaviour of real materials. Neglecting an anomalous behaviour we can expect that with respect to molecular effects *the instantaneous stiffness of crystalline solids increases under compression and decreases under tension.* This nonlinear elastic effect is responsible for many phenomena observed experimentally. For instance due to the different stress-strain response of the extension and compression regions, a single edge dislocation causes the volume expansion of crystal lattice [6, 11]. The asymmetry in the stress–strain response appears also in the form of negative values of third-order elastic constants measured experimentally for many real crystal structures [13, 15, 16]. Thus, applying elastic constitutive models which behave just conversely (St.-Venant–Kirchhoff, Biot) to the real material, can be the cause of many undesirable effects such as improper proportion between stress values and sizes of extension and compression regions around

a single edge dislocation which causes positive or negative volume expansion induced by edge dislocations in elastic continuum. Therefore, the use of new elastic and elastic-plastic constitutive models, whose behaviour could be more adapted to the nonlinear behaviour of real crystal structures, is desired.

2. Nonlinear continuum elasticity

According to the polar decomposition theorem, the deformation gradient $\mathbf{F}$ can be decomposed into the rotation tensor $\mathbf{R}$ and the left or right stretch tensor, $\mathbf{U}$ or $\mathbf{V}$, respectively, $\mathbf{F} = \mathbf{RU} = \mathbf{VR}$.

DEFINITION 1. *By general Lagrangian and Eulerian strain tensors we mean two tensor functions*

$$\widehat{\boldsymbol{\varepsilon}} \stackrel{\text{df}}{=} \mathcal{A} f(u_{\mathsf{i}})\, \mathbf{u}_{\mathsf{i}} \otimes \mathbf{u}_{\mathsf{i}} \qquad \textit{and} \qquad \boldsymbol{\varepsilon} \stackrel{\text{df}}{=} f(v_{\mathsf{i}})\ \mathbf{v}_i \otimes \mathbf{v}_{\mathsf{i}}, \tag{2.1}$$

where $u_{\mathsf{i}}, \mathbf{u}_{\mathsf{i}}, v_{\mathsf{i}}, \mathbf{v}_{\mathsf{i}}$ denote respectively i-th eigenvalues and eigenvectors of the right and left stretch tensors, while $f(x) : R^+ \ni x \to f \in R$ denotes an arbitrarily chosen C^1 monotonically increasing function which satisfies the conditions $f(x)|_{x=1} = 0$ and $\dfrac{df(x)}{dx}\Big|_{x=1} = 1$.

This definition includes the well-known family of strain measures noted first in [10]

$$\widehat{\boldsymbol{\varepsilon}} = \frac{1}{m}(\mathbf{U}^m - \mathbf{1}) \qquad \text{and} \qquad \boldsymbol{\varepsilon} = \frac{1}{m}(\mathbf{V}^m - \mathbf{1}), \tag{2.2}$$

and many others. It can be proved that to balance the energy for an arbitrarily chosen deformation process, the Cauchy stress has to be governed by the following equation:

$$\boxed{\boldsymbol{\sigma} = \mathbf{R}\left(\widehat{\boldsymbol{\mathcal{A}}} : \widehat{\rho}\frac{\partial \psi}{\partial \widehat{\boldsymbol{\varepsilon}}}\right)\mathbf{R}^T \det\mathbf{F}^{-1},} \tag{2.3}$$

where the fourth-order tensor $\widehat{\boldsymbol{\mathcal{A}}}$ decomposed in the vector basis $\{\mathbf{u}_{\mathsf{K}}\}$ consisting of the eigenvectors of right stretch tensor is represented by the following non-vanishing components:

$$\widehat{\mathcal{A}}_{\mathsf{IJIJ}} = \widehat{\mathcal{A}}_{\mathsf{IJJI}} = \begin{cases} \delta_{\mathsf{IJ}}\, u_{\mathsf{I}} f'(u_{\mathsf{I}}) & \text{for } u_{\mathsf{I}} = u_{\mathsf{J}}, \\ \dfrac{u_{\mathsf{I}} u_{\mathsf{J}}[f(u_{\mathsf{I}}) - f(u_{\mathsf{J}})]}{u_{\mathsf{I}}^2 - u_{\mathsf{J}}^2} & \text{for } u_{\mathsf{I}} \neq u_{\mathsf{J}}, \end{cases} \tag{2.4}$$

where $\widehat{\rho} = \rho \det \mathbf{F}$, $f'(u_\mathrm{I}) = \left.\dfrac{df(u)}{du}\right|_{u=u_\mathrm{I}}$, [4]. Let us consider the hyperelastic material governed by the following constitutive equation stated for the specific strain energy

$$\psi = \frac{1}{2\widehat{\rho}} \widehat{\boldsymbol{\varepsilon}} : \widehat{\mathbf{c}} : \widehat{\boldsymbol{\varepsilon}} \tag{2.5}$$

where $\widehat{\mathbf{c}}$ is the fourth-order tensor of elastic stiffness. Substitution into (2.3) leads to

$$\boldsymbol{\sigma} = \mathbf{R}(\widehat{\boldsymbol{\mathcal{A}}} : \widehat{\mathbf{c}} : \widehat{\boldsymbol{\varepsilon}})\mathbf{R}^T \det \mathbf{F}^{-1}. \tag{2.6}$$

This constitutive model based on the generalized strain measure takes into account the most of the well-known anisotropic elastic models. Obviously, the models which do not satisfy the energy conservation law, like hypoelastic models, are out of our consideration.

3. Interatomic potentials

Recently a wide group of interatomic potentials are used in the computation materials science. Below, we present in brief the mathematical foundation of a few empirical potentials.

Embedded Atom Method. The Embedded Atom Method has been proposed by M. I. BASKES and M. S. DAW in 1984 [3]. The EAM is using the density functional theory. In this model, the energy required to place an atom in crystal lattice is a function of electron density in the desired place. This method is using two-body interactions so it is a central a forces method. This allows to calculate lattice relaxation and many properties of large sets of atoms. The fundamental equations for EAM are

$$E_{\mathrm{tot}} = \sum_i F_i(\rho_{h,i}) + \frac{1}{2}\sum_{i,j} \phi_{i,j}(R_{i,j}), \tag{3.1}$$

$$\rho_{h,i} = \sum_{j(\neq i)} \rho_j^a(R_{ij}), \tag{3.2}$$

where E_{tot} is total internal energy, $\rho_{h,i}$ is closely approximated by a sum of atomic densities ρ^a of the constituents [i.e. $\rho_{h,i,}$], f_i is electron density of atom j as a function of distance from its center, R_{ij} is distance between atoms i and j, $F_i(\rho_{h,i})$ is energy of embedded atom i for electron density $\rho_{h,i}$ and $\phi_{i,j}$ is the short range (doubly screened) pair potential. This potential looks quite simple but the results obtained using it are very close to those obtained experimentally [3, 5].

All parameters are more precisely discussed by authors of this potential. The numerical problem in applying this potential is that it requires to calculate the interactions of all atoms with each other – that gives a huge number of equations to process. Two other presented potentials have a cut-off parameter which allows to limit the number of interacting atoms to those within cut-off range.

Tersoff potential is more advanced than two-body potentials. The Tersoff potential depends not only on atomic distances but also on the angle between three atoms (two bindings) [8]. That makes this potential more flexible and accurate in calculations, but it makes it harder to adapt to numerical calculations. The geometric term which contains information about the angle θ between two bindings is very important. This angle limits the number of atomic positions – without this term the number of possible positions is almost unlimited and does not correlate with physical reality (the angle between e.g. Ga–As and As–Ga in a crystal is known exactly). The energy function

$$E = \sum_i \frac{1}{2} \sum_{j \neq i} V_{ij}, \tag{3.3}$$

where V_{ij} is the energy of bindings between i-atom and j-atom in a crystal,

$$V_{ij} = f_C(r_{ij})[f_B(r_{ij}) + b_{ij} f_A(r_{ij})]. \tag{3.4}$$

Functions f_A and f_B are the attractive and repulsive parts of potentials for a pair of atoms. The function f_C is responsible for limiting the length of bond and is a smooth cutoff function. The parameters R and D are chosen in order to limit the interactions to first-neighbour shell only. The functions are described below:

$$f_A(r) = -Be^{-\lambda_2 r}, \tag{3.5}$$

$$f_B(r) = Ae^{-\lambda_1 r}, \tag{3.6}$$

$$f_C(r) = \begin{cases} 1 & \text{for} \quad r < R - D, \\ \dfrac{1}{2} - \dfrac{1}{2} \sin \dfrac{\pi(r-R)}{2D} & \text{for} \quad R - D < r < R + D, \\ 0 & \text{for} \quad r > R + D, \end{cases} \tag{3.7}$$

$$b_{ij} = (1 + \beta^n {\xi_{ij}}^n)^{-1/2n}, \tag{3.8}$$

$$\xi_{ij} = \sum_{k \neq (i,j)} f_C(r_{ik}) g(\theta_{ijk}) e^{{\lambda_3}^3 (r_{ij} - r_{ik})^3}. \tag{3.9}$$

The b_{ij} term is responsible for the strength of bonds. In this case the bond strength depends on local environment and is lower when the number of neighbours is relatively high. This potential is based on the Morse interactions.

The parameters should be chosen to fit the theoretical and experimental data obtained for realistic and hypothetical crystal configurations, e.g. the cohesive energy of several high-symmetry bulk structures, the lattice constant and bulk modulus of the researched crystal lattice [14].

Stillinger–Weber potential [12], its energy function comprises both two- and three-atom contributions which make it possible to describe complex deformations in crystals more accurately than in the case of potentials based only on two-atomic interactions. Any interatomic energy function describing interactions between N atoms can be simplified to one-body, two-body, three-body etc. interactions as it is presented in the following equation:

$$\Psi(1,\ldots,N) = \sum_i v_1(i) + \sum_{\substack{i,j \\ i<j}} v_2(i,j) + \sum_{\substack{i,j,k \\ i<j<k}} v_3(i,j,k) + \ldots + v_N(1,\ldots,N). \tag{3.10}$$

The potential v_1 stands for a single particle in the system. This part will be neglected because it is not considered in our discussion. It is important that the component functions v_n should quickly tend to zero with increasing value of n. To this end the Stillinger–Weber potential is approximated only by v_2 and v_3 functions, that is two-body and three-body interactions. The potential is based on the well-known Lennard–Jones potential, which was assumed for noble gases description; however, it is unusable for semiconductors due to the lack of fitting parameters. The partial energy functions v_2 and v_3 are introduced as follows

$$v_2(r_{ij}) = \epsilon f_2(r_{ij}/\sigma) \quad \text{and} \quad v_3(\mathbf{r}_i,\mathbf{r}_j,\mathbf{r}_k) = \epsilon f_3(\mathbf{r}_i/\sigma,\mathbf{r}_j/\sigma,\mathbf{r}_k/\sigma), \tag{3.11}$$

where ϵ is chosen to give f_2 depth -1, and σ is chosen to make $f_2(2^{1/6})$ vanish. The f_2 is a function only of the scalar distance, but f_3 must possess full translational and rotational symmetry.

Finally the two-body part of Stillinger–Weber potential takes the following form:

$$f_2(r) = \begin{cases} A(Br^{-p} - r^{-q})e^{\frac{1}{r-a}} & \text{for} \quad r < a, \\ 0 & \text{for} \quad r \geq a, \end{cases} \tag{3.12}$$

where the constants A, B, p have to be positive. This potential is also automatically cut off when $r = a$, without any discontinuities in any r derivative, which makes it very useful in any molecular dynamics simulations.

The same cut-off condition has to be held in the three-body interactions

$$f_3(\mathbf{r}_i,\mathbf{r}_j,\mathbf{r}_k) = h(\mathbf{r}_{ij},\mathbf{r}_{ik},\Theta_{jik}) + h(\mathbf{r}_{ji},\mathbf{r}_{jk},\Theta_{ijk}) + h(\mathbf{r}_{ki},\mathbf{r}_{kj},\Theta_{ikj}), \tag{3.13}$$

where Θ_{ijk} denotes the angle between r_i and r_k subtended at vertex i. The function h has two parameters $(\lambda, \gamma > 0)$, it takes the form

$$h(\mathbf{r}_{ij}, \mathbf{r}_{ik}, \Theta_{jik}) = \begin{cases} \lambda e^{\frac{\gamma}{r_{ij}-a}+\frac{\gamma}{r_{ik}-a}} \left(\cos\Theta_{jik} + \frac{1}{3} \right) & \text{for} \quad r_{ij}, r_{ik} < a, \\ 0 & \text{for} \quad r \geq a. \end{cases}$$

For this part the Θ parameter is very important; it gives us information about the crystal deformation. When Θ is such that $\cos\Theta = -1/3$, then the three-body potential vanishes, which is because of the perfect tetrahedral angle $\cos\Theta = -1/3$. This shows that in an undeformed state this potential is based only on two-body interactions.

Table 1. Parameters assumed for the Stillinger–Weber potential.

	ε (eV)	σ (nm)	a	A	B	λ	υ
GaAs	1.409	0.210	1.794	8.513	0.782	27.0	1.0
CdTe	1.088	0.228	1.863	8.582	0.993	27.0	1.20

We have used parameters determined in [2] for GaAs. The parameters $A, B, p, q, a, \lambda, \gamma$ have been determined on the basis of many conditions. One of them is crystal's minimal energy in undeformed state. The second condition arises from experimental values of the elastic constants and the third one from the temperature of melting point and other similar constants. Some constants are calculated using the *ab initio* methods for determining physical properties of atomic bonds. In addition we compared the crystal's energy, calculated with the Stillinger–Weber potential, response on stretching with hyperelastic models based on generalized strain models which is shown in Fig. 1.

To find the stress-strain response of atomic structure the energy of which is governed by a given interatomic potential, we have applied the following relation yielding from the strain energy balance:

$$\widehat{\boldsymbol{\sigma}}_I = \widehat{\rho} \frac{\partial \Psi}{\partial \mathbf{F}}, \tag{3.14}$$

where $\widehat{\boldsymbol{\sigma}}_I$ denotes the first Piola–Kirchhoff stress tensor while Ψ means the crystal's specific free energy (per unit mass). The energy depends on distances and positions between all the atoms in the crystal, i.e. $\Psi = \Psi(\mathbf{r}_1, \ldots, \mathbf{r}_N)$. Assuming that the current position vector $\mathbf{r}_i$ depends on the deformation gradient $\mathbf{F}$ and on the reference position vector $\mathbf{R}_i$, we find

$$\frac{\partial \Psi}{\partial \mathbf{F}} = \sum_i \left(\frac{\partial \Psi}{\partial \mathbf{r}_i} \frac{\partial (\mathbf{F}\mathbf{R}_i)}{\partial \mathbf{F}} \right) = \sum_i \left(\frac{\partial \Psi}{\partial \mathbf{r}_i} \otimes \mathbf{R}_i \right), \tag{3.15}$$

where $\mathbf{r}_i = \mathbf{F}\mathbf{R}_i$. Substituting (3.15) into (3.14) we find the Cauchy stress tensor corresponding to the Stillinger–Weber potential

$$\boldsymbol{\sigma} = \widehat{\rho}\frac{\partial \Psi}{\partial \mathbf{F}}\mathbf{F}^T \det \mathbf{F}^{-1}. \tag{3.16}$$

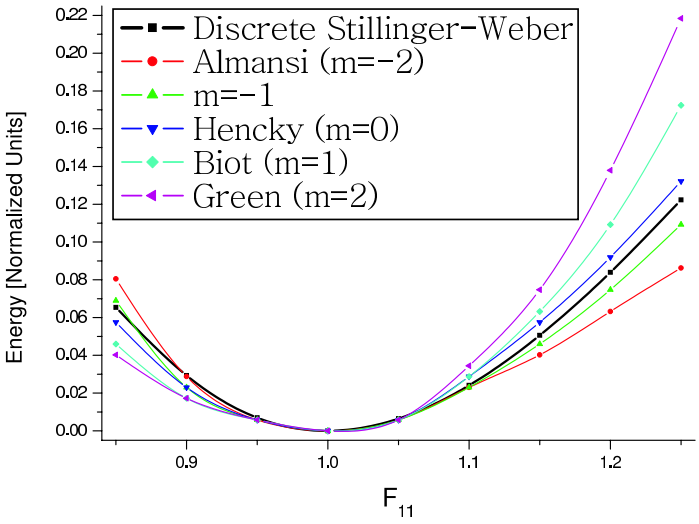

FIG. 1. Energy of hyperelastic models based on generalized strain models versus discrete Stillinger–Weber potential model in uniaxial stretch test.

The method described above is very similar to the method used by [17]. Because the calculation of stress on the basis of numerical differentiation of all two- and three-atomic terms over the deformation process turned out to be very time-consuming, the Stillinger–Weber potential model was replaced by a nonlinear hyperelastic constitutive model based upon a non-monotonic (pseudo-strain) functions. Finally, the functions below will describe the continuized Stillinger–Weber model.

$$\widehat{\boldsymbol{\varepsilon}} = \sum_{i=1}^{3} \ln u_{\mathrm{i}}\; e^{-\frac{n}{2}(u_{\mathrm{i}}^2-1)}\; \mathbf{u}_{\mathrm{i}} \otimes \mathbf{u}_{\mathrm{i}}, \tag{3.17}$$

$$\boldsymbol{\varepsilon} = \sum_{i=1}^{3} \ln v_{\mathrm{i}}\; e^{-\frac{n}{2}(v_{\mathrm{i}}^2-1)}\; \mathbf{v}_{\mathrm{i}} \otimes \mathbf{v}_{\mathrm{i}}, \tag{3.18}$$

where n is a strain parameter. In our research we have found parameter n by fitting the above functions to discrete Stillinger–Weber potential. The fitting procedure shows that the parameter n should be 0.57 for GaAs crystal lattice. We didn't fit the n parameter for CdTe or ZnTe. The results of using such a

continuized potential function for GaAs are presented in Fig. 2. This fitted model differs from the discrete Stillinger–Weber potential, the difference is about 3%. The stretching test was performed with atoms able to reorganize themselves.

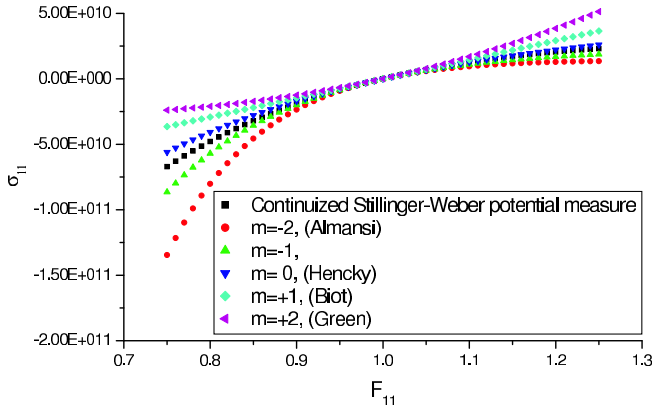

FIG. 2. Stress of hyperelastic models based on generalized strain models versus continuized Stillinger–Weber potential model in uniaxial stretch test.

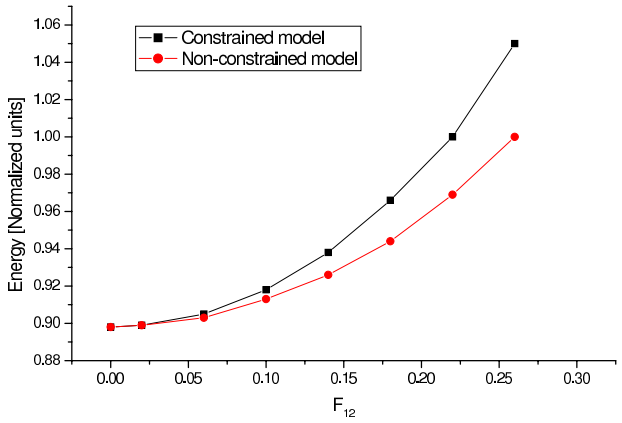

FIG. 3. Stress-strain comparison of the considered constrained and non-constrained model for the simple shear test.

We made also a shearing test for the Stillinger–Weber potential model. The shear test plot is a comparison between a model with atoms allowed to reorganize and find their local energy minima and another one where atoms are placed with no possibility to move.

4. Quantum dot calculations example

We have applied the discrete Stillinger–Weber potential with special subroutines to FEM solver, namely FEAP [18]. Here we must explain that although the algorithm is using a FEM solver, it is not the Finite Element Method – there are no finite elements.

In our approach we have used subroutines describing two- and three-body interaction terms. The fundamental difference between our method and FEM is that our, let's say, pseudo-elements do not contain continuous distributions of mass and stress/forces within elements, but they are based on the energy balance of discrete atoms situated in the mesh nodes, which satisfy the motion equation

$$m_n \ddot{r}_n = f_n, \tag{4.1}$$

where the nodal forces f_n are determined as a superposition of elemental forces

$$f_n^2 = \frac{\partial v_2}{\partial r_n} \qquad \text{and} \qquad f_n^3 = \frac{\partial v_3}{\partial r_n} \tag{4.2}$$

corresponding directly to the two- and three-body terms of energy, v_2 and v_3, according to (17). In other words, in the classical FEM the energy, mass and forces are continuously distributed within elements, while in our approach there are no continuous distributions over the two- and three-body pseudo-elements. Such approach allows us to link these pseudo-elements with the classical solver of FEM. Such attempt doesn't require any changes in the FEAP solver.

The mesh, similar to the FE mesh, is only a graphic representation of all possible connections and data needed to calculate the interaction between atoms. The algorithm is capable of calculating dynamic (time-dependent) or static problems. The material distribution is assumed for quantum dot structures observed on HRTEM experimental images [7]. In this example we applied CdTe in ZnTe quantum dot atoms positions to the prepared program which generates mesh of pseudo-elements. The generator produces a block of sphallerite structure of desired size and shape or uses an input file where the atoms position were stored (e.g. Zn, Te or Cd). The Stillinger–Weber potential which is applied in our pseudo-elements recognizes the bond type and the atoms by recognizing the material number (e.g. Cd–Te material has the number "1" and Zn–Te has the number "2"). The quantum dot was composed of 40 300 atoms – to limit the calculation time and conserve the computer memory we applied the so-called multipoint displacement boundary conditions on each boundary plane of our block chosen for calculation. These conditions correspond to the assumption that the quantum dot is not alone in the bulk material but is surrounded by other quantum dots of the same shape and size what also required setting the boundary

conditions on external walls of our material. Finally the problem was limited to only 10 075 atoms. In the presented example we have calculated the static problem – time-independent. The assumed quantum dot material decomposition is shown in Fig. 4.

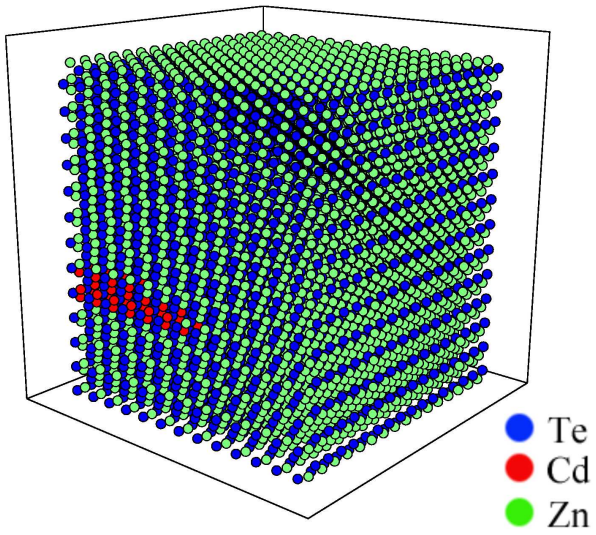

FIG. 4. Assumed material decomposition in quantum dot quarter.

The obtained atom displacements, Fig. 5, were compared with similar quantum dot calculated with FEM, and they were very similar both in the shape and the displacements. In initial state of the performed simulation both structures of quantum dot and the surrounding region have the same lattice constant – ZnTe lattice constant. Because CdTe has a larger lattice constant than ZnTe, we expected that the quantum dot region will extend to reach the CdTe lattice constant. Such extension can be noticed in Fig. 5 presenting the directions of extension X, Y and Z. We can notice that the largest displacements are in pictures presenting X plane (almost 0.22 nm) and Z plane (0.28 nm), what is caused by periodic boundary conditions. The block of crystal presented here is a simulation of an infinite line of quantum dots in Y direction, so the last row of atoms in Y direction has been disabled to move along the Y axis – in real structure just behind the last row of atoms begins the next similar quantum dot which interacts in opposite direction [7]. These results can be later easily applied to the HRTEM image simulation program allowing to verify and reconstruct the quantum structures observed in laboratory conditions. Parameters for the Stillinger–Weber potential used in these calculation were taken from [9, 2].

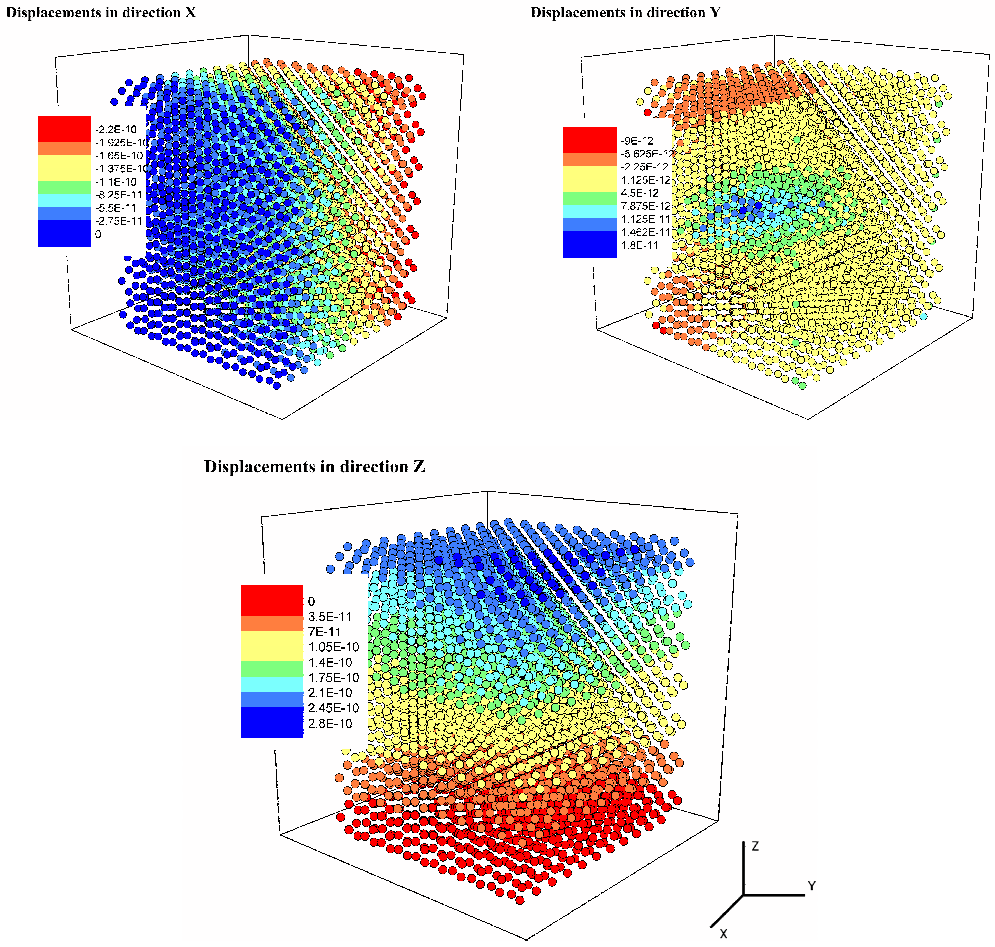

FIG. 5. Displacements resulting from the performed calculations.

5. Conclusion

In the hyperelasticity based upon general strain measure, the fundamental question arises: which of the finite strain measures is the best one? The choice of the given measure is responsible for the higher order elastic effects. For example, the third-order elastic constants depend very strongly on the strain measure choice, see [4]. In this paper, we have shown that the nonlinear elastic behaviour of one of the most popular interatomic potentials used in MD simulations, namely the behaviour of the Stillinger–Weber potential, is closest to the behaviour of the first-order hyperelastic models based upon the strains corresponding to the strain parameter between –1 and 0. This means that the first-order anisotropic

hyperelasticity based upon the strain $\boldsymbol{\varepsilon} = \ln \mathbf{U}$ or $\boldsymbol{\varepsilon} = -\mathbf{U}^{-1} + \mathbf{1}$ gives approximately the same extension/compression asymmetry in elastic behaviour as that obtained by physicists with the use of interatomic potential like the Stillinger–Weber one. Recently, it has been used in the majority of MD simulations carried out for semiconductor nanostructures. Obviously, our comparison concerned only the elastic behaviour in the uniaxial deformation range in which the interatomic potential was able to hold a stable GaAs atomic structure in the approximately uniform deformation state.

Acknowledgment

This work was supported by the State Committee for Scientific Research (KBN) in Poland under Grants No. 7 T07A 004 16 and 7 T07A 01517.

References

1. L. ANAND, *On H. Hencky's approximate strain-energy function for moderate deformations*, Transactions of ASME, **46**, 78–82, 1979.
2. J. E. ANGELO and M. J. MILLS, *Investigations of the misfit dislocation structure at a CdTe(001)/GaAs(001) interface using Stillinger-Weber potentials and high-resolution transmission electron microscopy,* Philosophical Magazine A, **72**, 3, 635–649, 1995.
3. M. I BASKES and M. S. DAW, *Embedded-atom-method: Derivation and application to impurities, surfaces, and other defects in metals*, Phys. Rev. B, **29**, 6443, 1984.
4. P. DŁUŻEWSKI, *Anisotropic hyperelasticity based upon general strain measures*, Journal of Elasticity, **60**, 2, 119–129, 2000.
5. M. I. FOILES, S. M. BASKES and M. S. DAW, *Embedded-atom-method functions for the fcc metals Cu, Ag, Au, ni, Pd, Pt, and their alloys*, Phys. Rev. B., **33**, 7983, 1986.
6. M. J. HORODON and B. L. AVERBACH, Acta Metallurgica, 9, 247, 1961.
7. E. SOBCZAK, A. SZCZEPANSKA, S. MACKOWSKI, T. WOJTOWICZ, G. KARCZEWSKI, J. KOSSUT, S. KRET, P. DLUZEWSKI and P. RUTERANA, *Electron microscopy study of ZnTe/CdTe superlattice with high density of quantum dots*, Mat. Res. Soc. Symp. Proc., 642, 2001.
8. D. RAABE, *Computational material science. The simulations of materials and properties*, Wiley-VCH, Weinheim 1998.
9. D. KIRMSE, H. SCHNEIDER, R. SCHEERSCHMIDT, K. CONRAD and W. NEUMANN, *Electron microscope characterization of CdSe/ZnSe quantum dots based on molecular dynamics structure relaxations*, Ultramicroscopy, **81**, 289–300, 200.
10. B. R. SETH, *Generalized strain measure with applications to physical problems*, [in:] M. REINER and D. ABIR [Eds.], *Second-order effects in elasticity, Plasticity and Fluid Dynamics*, Pergamon Press Oxford 1964. Proc. Int. Symp., April 23–27, Haifa 1962.
11. F. SPAEPEN, *Interfaces and stresses in thin films*, Acta Materialia, **48**, 31–42, 2000.

12. F. H STILLINGER and T. A. WEBER, *Computer simulation of local order in condensed phases of silicon*, Physical Review B, **31**, 8, April 15 1985.

13. C TEODOSIU, *Elastic models of crystal defects*, Springer-Verlag and Editura Academiei, Berlin and Bucureşti 1982.

14. J. TERSOFF, *Empirical interatomic potential for carbon, with applications to amorphous carbon*, Phys. Rev. Lett., **61**, 2879, 1988.

15. S. N. VAIDYA and G. C. KENNEDY, *Compressibility of 18 metals to 45kb*, J. Phys. Chem. Solids, **31**, 2329–2345, 1970.

16. S. N. VAIDYA and G. C. KENNEDY, *Compressibility of 22 elemental solids to 45kb*, J. Phys. Chem. Solids, **33**, 1377–1389, 1972.

17. K. YASHIRO and Y. TOMITA, *Local lattice instability at dislocation nucleation and motion*, J. Phys. IV France, 11, PR5–3, 2001.

18. O. C. ZIENKIEWICZ and R. J. TAYLOR, *The finite element method*, McGraw-Hill, London 1991.

Received January 22, 2003.